

# Quantitative Formulation of Average Force in Amplitude-Modulation Atomic Force Microscopy

Kenichi Umeda<sup>1,2</sup>, Karen Kamoshita<sup>3</sup>, and Noriyuki Kodera<sup>1,4</sup>

<sup>1</sup> *Nano Life Science Institute (WPI-NanoLSI),*

*Kanazawa University, Kakuma-machi, Kanazawa, Ishikawa, 920-1192, Japan.*

<sup>2</sup> *PRESTO/JST, 4-1-8 Honcho, Kawaguchi, Saitama 332-0012, Japan.*

<sup>3</sup> *School of Mathematics and Physics, College of Science and Engineering,*

*Kanazawa University, Kakuma-machi, Kanazawa, Ishikawa, 920-1192, Japan.*

<sup>4</sup> *CREST/JST, 4-1-8 Honcho, Kawaguchi, Saitama 332-0012, Japan.*

Corresponding Authors

Dr. Kenichi Umeda (E-mail: [umeda.k@staff.kanazawa-u.ac.jp](mailto:umeda.k@staff.kanazawa-u.ac.jp))

Prof. Noriyuki Kodera (E-mail: [nkoder@staff.kanazawa-u.ac.jp](mailto:nkoder@staff.kanazawa-u.ac.jp))

## Abstract

Amplitude-modulation (tapping-mode) atomic force microscopy (AM-AFM) is a technique for obtaining surface topographic images at the atomic or molecular-scale by detecting changes in the cantilever oscillation amplitude. Since it can operate in air or liquid conditions, it has contributed to various material research fields. However, it remains unclear why the tip-sample interaction force estimated from an experimental amplitude value is substantially greater than the actual molecular binding force, despite the successful visualization of molecular dynamics. Here, we performed a theoretical analysis to tackle this question. We show that in general AM-AFM measurements, the cantilever is excited at the resonance slope whereas the conventional equation is only valid for excitation exactly at the resonance frequency. We then derive a force conversion equation for an arbitrary excitation frequency and found that the conventional equation overestimates the actual force by about five times. The theory derived here can be used for diverse AM-AFM applications, and is useful in many fields of material research.

## 1. Introduction

Amplitude-modulation (tapping-mode) atomic force microscopy (AM-AFM), a type of dynamic-mode AFM, is a technique that allows imaging at the atomic and molecular scale with minimal perturbation. It has been used in various material science researches, e.g., electrochemistry [1], electronics [2-4], biology [2,5-7], and polymer [2,3,8], because it operates in liquid as well as ambient conditions. In particular, this technique has contributed to the bio-AFM field [9] because it is a unique technique that allows visualization of living biological samples at the submolecular scale. Recently, high-speed AFM (HS-AFM) has been developed to visualize dynamics on the tens of milliseconds via increasing the bandwidth of AM-AFM devices [10,11]. This new application has facilitated great advances in basic life science [5,10-15].

Over the 40-year history of AM-AFM, most of its fundamental principles have been clarified [16-20]. In particular, since AM-AFM detects the tip-sample interaction force as a change in the cantilever amplitude, a theoretical equation for converting the amplitude value to average force was already proposed in the early days of AM-AFM [17,18]. Although this equation is widely known, the force is commonly overestimated compared to the actual molecular binding force, which is typically 5–20 pN [21,22]. Nevertheless, molecular dynamics can be visualized without disturbing the molecular structure through excessive tip-sample force. This anomaly has remained unexplained and unaddressed by the HS-AFM community.

Force magnitude accuracy is often important in AM-AFM experiments. For example, there are proteins that undergo structural changes in response to mechanical stimuli [5], and molecules whose structure is easily perturbed or denatured by the tip interaction during the imaging [6,12,23]. Furthermore, experiments in which supramolecular complexes are manipulated or disassembled via the tip interaction are also reported [9,13,15]. If quantitative estimation of the tip-sample force

becomes feasible, we could gain more detailed insight into the fragility and binding strength of these molecules and also contribute to optimizing the feedback parameters required for non-destructive imaging of fragile molecules.

In this study, we performed a theoretical analysis which revealed that the estimated average force depends strongly on the excitation frequency. We also derived a quantitative conversion equation to estimate tip-sample force from the amplitude value, addressing one of the longstanding enigmas in the field of AM-AFM. The theoretical formulation shown here is expected to have a major impact on various material research fields, particularly in the bio-AFM field, where observations must be made with as little force as possible.

## 2. Conversion from Amplitude to Force

In AM-AFM, to accurately reconstruct the average force, 3D volume data of the amplitude and phase signals simultaneously acquired from a far distance from the surface is required [19,24,25]. Such experiments are time consuming, and therefore not compatible with high-speed measurements. Thus, in previous studies, a more simple force conversion method has been proposed based on a large-amplitude approximation that requires only the amplitude value as a variable [17,18]. This theoretical formulation is based on excitation at the resonance frequency following another dynamic-mode AFM, frequency-modulation AFM [26]. However, in AM-AFM, the maximum force sensitivity can be obtained by driving the cantilever at the resonance slope [20]. Therefore, here we derive a theoretical equation that can be applied to an arbitrary excitation frequency ( $f_{\text{drive}}$ ).

The equation of motion of the cantilever based on a simple harmonic oscillator (SHO) model is expressed as follows:

$$m_{\text{cl}} z''(t) + \frac{\omega_0 m_{\text{cl}}}{Q_{\text{cl}}} z'(t) + k_z z(t) = \underbrace{F_{\text{drive}} \cos(\omega_{\text{drive}} t)}_{\text{External driving force}} + \underbrace{F_{\text{ts}}(z(t), z'(t))}_{\text{Tip-sample force}}, \quad (1)$$

where  $m_{\text{cl}}$ ,  $\omega_0 (= 2\pi f_0)$ ,  $Q_{\text{cl}}$ ,  $k_z$ ,  $F_{\text{drive}}$ , and  $\omega_{\text{drive}} (= 2\pi f_{\text{drive}})$  are the effective mass, eigenfrequency, quality factor, spring constant, driving force, and driving frequency of the cantilever, respectively; and  $z(t)$  is the displacement of the cantilever at time  $t$ . Hereafter, we denote  $f$  and  $\omega (= 2\pi f)$  as a certain frequency and its angular frequency, respectively.

Normally, the distance dependence of the tip-sample interaction is nonlinear; however, when the interaction is relatively small, the harmonic components can be ignored. By the following equation assuming a steady-state oscillation,  $z(t)$  can be expressed as

$$z(t) \approx \langle z \rangle + A_{\text{cl}} \cos(\omega_{\text{drive}} t + \phi_{\text{drive}}), \quad (2)$$

where  $\langle z \rangle$ ,  $A_{\text{cl}}$ , and  $\phi_{\text{drive}}$  are the average position of the cantilever displacement, oscillation

amplitude, and phase delay in the excitation system, respectively. Using the Fourier series of the tip-sample interaction, we solve this equation to obtain the transfer function  $G_{cl}$  [27];

$$G_{cl}(\omega) = \frac{1}{k_z} \frac{1}{\left(1 - \tilde{\omega}_{drive}^2 - I_{even}(z, A_{cl})\right) + i\left(\tilde{\omega}_{drive} / Q_{cl} + I_{odd}(z, A_{cl})\right)}, \quad (3)$$

where  $\tilde{\omega}_{drive}$  is defined as a normalized  $f_{drive}$  as follows:

$$\tilde{\omega}_{drive} = \frac{\omega_{drive}}{\omega_0} = \frac{f_{drive}}{f_0}, \quad (4)$$

and  $I_{even}$  and  $I_{odd}$  represent the in-phase and out-of-phase terms of the Fourier components, reflecting conservative forces and energy dissipation, respectively [19,27,28], and are expressed as,

$$\begin{aligned} I_{even}(z, A_{cl}) &= \frac{2f_{drive}}{k_z A_{cl}} \int_0^{1/f_{drive}} F_{ts}[z(t), z'(t)] \cos(\omega_{drive}t + \phi_{drive}) dt \\ &= \frac{2}{k_z A_{cl}^2} \langle F_{ts} \cdot z \rangle \propto \Delta f, \end{aligned} \quad (5)$$

$$\begin{aligned} I_{odd}(z, A_{cl}) &= \frac{2f_{drive}}{k_z A_{cl}} \int_0^{1/f_{drive}} F_{ts}[z(t), z'(t)] \sin(\omega_{drive}t + \phi_{drive}) dt \\ &= -\frac{1}{\pi f_{drive} k_z A_{cl}^2} \langle F_{ts} \cdot z' \rangle, \end{aligned} \quad (6)$$

where  $F_{ts}$  is the tip-sample interaction force. By following the original definition by Dürig et al. [29], we defined them as even or odd relative to the tip trajectory. Moreover, the amplitude and phase of  $G_{cl}$  are calculated as

$$\begin{aligned} A_{cl}(\tilde{\omega}_{drive}) &= |G_{cl}(\tilde{\omega}_{drive})| F_{drive} \\ &= \frac{A_0}{\sqrt{\left(1 - \tilde{\omega}_{drive}^2 - I_{even}(z, A_{cl})\right)^2 + \left(\tilde{\omega}_{drive} / Q_{cl} + I_{odd}(z, A_{cl})\right)^2}}, \end{aligned} \quad (7)$$

$$\phi_{cl}(\tilde{\omega}_{drive}) = \angle G_{cl}(\tilde{\omega}_{drive}) = \tan^{-1} \left( \frac{\tilde{\omega}_{drive} / Q_{cl} + I_{odd}(z, A_{cl})}{1 - \tilde{\omega}_{drive}^2 - I_{even}(z, A_{cl})} \right), \quad (8)$$

respectively, where  $A_0$  represents the amplitude at  $\tilde{\omega}_{drive} = 0$ . In the absence of the tip-sample interaction,  $A_{cl}$  is expressed by

$$A_{cl}(\tilde{\omega}_{drive}, I_{even} = I_{odd} = 0) = \frac{A_0}{\sqrt{\left(1 - \tilde{\omega}_{drive}^2\right)^2 + \left(\tilde{\omega}_{drive} / Q_{cl}\right)^2}}, \quad (9)$$

Fig. 1(a,b) shows the frequency characteristics of amplitude value as a function of  $I_{\text{even}}$  and  $I_{\text{odd}}$ . For the repulsive force ( $I_{\text{even}} < 0$ ), in Fig. 1(a), a positive resonance frequency shift and a reduction in the overall excitation efficiency occur because the effective  $k_z$  of the system increases. In contrast, for the attractive force ( $I_{\text{even}} > 0$ ), a negative frequency shift and an increase in the overall excitation efficiency occur because the effective  $k_z$  decreases. Furthermore, the effective  $Q_{\text{cl}}$  increases for the repulsive force ( $I_{\text{even}} < 0$ ), which makes the amplitude change at the resonance peak less sensitive to the tip-sample force. Additionally, in Fig. 1(b), as  $I_{\text{odd}}$  increases,  $Q_{\text{cl}}$  and the overall excitation efficiency decreases, but the resonance frequency shift does not occur. In other words, the maximum sensitivity for  $I_{\text{odd}}$  can be obtained by exciting at the frequency near the resonance peak.

Fig. 1(c,d) shows an enlarged view of the frequency characteristics near the resonance. It is well known that when  $Q_{\text{cl}}$  is sufficiently large, the maximum amplitude appears exactly at  $f_0$ . However, as seen here, when  $Q_{\text{cl}}$  becomes significantly low, the resonance peak frequency ( $f_{\text{peak}}$ ) slightly shifts negative relative to  $f_0$ . The analytical solution for  $f_{\text{peak}}$  can be found by setting the derivative of  $A_{\text{cl}}$  (Eq.(9)) to zero, as follows:

$$\frac{\partial A_{\text{cl}}(\tilde{\omega}_{\text{drive}})}{\partial \tilde{\omega}_{\text{drive}}} = A_0 \frac{\tilde{\omega}_{\text{drive}} [2(1 - \tilde{\omega}_{\text{drive}}^2) - 1/Q_{\text{cl}}^2]}{[(1 - \tilde{\omega}_{\text{drive}}^2)^2 + (\tilde{\omega}_{\text{drive}}/Q_{\text{cl}})^2]^{3/2}} = 0. \quad (10)$$

Solving this equation, we obtain the expression of normalized  $f_{\text{peak}}$  ( $\tilde{\omega}_{\text{peak}}$ ) as follows:

$$\tilde{\omega}_{\text{peak}} = \frac{\omega_{\text{peak}}}{\omega_0} = \frac{f_{\text{peak}}}{f_0} = \sqrt{1 - \frac{1}{2Q_{\text{cl}}^2}}. \quad (11)$$

In Fig. 1(c), the amplitude value tends to effectively decrease with reducing  $I_{\text{even}}$  when excited at  $f_{\text{peak}}$  or lower. However, even when  $I_{\text{even}}$  is changed, the amplitude value is almost unchanged at  $f_0$  and rather increases at a frequency higher than  $f_0$ . In contrast, in Fig. 1(d), when  $I_{\text{odd}}$  is changed, the amplitude value decreases regardless of  $f_{\text{drive}}$ , particularly, near  $f_{\text{peak}}$ .

This can be explained as follows. As AM-AFM is also known as the slope detection method [16,20,26], it has been theoretically clarified that the sensitivity of conservative forces,

which are reflected in the resonance frequency shift, is also maximized when the cantilever is excited at the MaxSlope frequency ( $f_{MS}$ ) where the slope of the resonance peak is maximum. In ambient conditions [4], the upper MaxSlope frequency ( $f_{UMS}$  in Fig. 1(c,d)) is normally excited to effectively detect the negative frequency shift due to attractive interactions, whereas in liquid conditions, the lower MaxSlope frequency ( $f_{LMS}$  in Fig. 1(c,d)) is excited to effectively detect the positive frequency shift due to repulsive interactions. Moreover, in liquids, excitation at a slightly lower off-resonance frequency is important not only to improve the sensitivity, but also to compensate for the slight negative shift of  $f_0$  due to the squeeze film effect during approach [30]. If the attractive and repulsive forces are switched during imaging, the amplitude would not decrease monotonically as the tip approaches, making imaging unstable [27,31]. For this reason, in liquid AM-AFM experiments, excitation at the lower MaxSlope frequency is normally used. In addition, most AM-AFM operation manuals also recommend for users to excite the cantilever at a slightly off-resonance frequency [32-36].

Particularly for HS-AFM experiments, most protein surfaces are relatively elastic, and imaging is performed with a small force of less than a few tens of pN; hence  $I_{odd}$  can be negligible compared to  $I_{even}$ . Furthermore, by normalizing the amplitude value when excited at  $f_{drive}$  in the absence of tip-sample interaction using  $A_{free}$ ,  $A_{cl}$  can be expressed as,

$$A_{cl}(\tilde{\omega}_{drive}) = A_{free} \sqrt{\frac{(1 - \tilde{\omega}_{drive}^2)^2 + (\tilde{\omega}_{drive} / Q_{cl})^2}{\left(1 - \tilde{\omega}_{drive}^2 - \frac{2}{k_z A_{cl}^2} \langle F_{ts} \cdot z \rangle\right)^2 + (\tilde{\omega}_{drive} / Q_{cl})^2}}. \quad (12)$$

When the oscillation amplitude is large and the tip is in contact with the sample for only a short time during one cantilever period, the large-amplitude approximation can be applied as follows [31]:

$$\lim_{A_{free} \rightarrow \infty} \langle F_{ts} \cdot z \rangle \approx -A_{cl} \langle F_{ts} \rangle. \quad (13)$$

By solving this equation for  $\langle F_{ts} \rangle$ , we obtain the force conversion equation at arbitrary  $f_{drive}$  as

$$\langle F_{ts} \rangle = \frac{k_z A_{free}}{2} \left[ -(1 - \tilde{\omega}_{drive}^2) \tilde{A}_{cl} + \sqrt{(1 - \tilde{\omega}_{drive}^2)^2 + (\tilde{\omega}_{drive} / Q_{cl})^2 (1 - \tilde{A}_{cl}^2)} \right], \quad (14)$$



where  $\tilde{A}_{cl}$  is the setpoint ratio (SPR), which is defined in turn as  $A_{cl}$  normalized by the free amplitude value  $A_{free}$ , and is expressed as:

$$\tilde{A}_{cl} = \frac{A_{cl}}{A_{free}} = \frac{A_{free} + \Delta A_{ts}}{A_{free}}, \quad (15)$$

where  $\Delta A_{ts}$  is the amplitude change due to the tip-sample interaction. By substituting  $\omega_0$  for  $\omega_{drive}$ , namely,  $\tilde{\omega}_{drive} = 1$ , we obtain the well-known conventional conversion equation as follows [5,8,10,13,18]:

$$\langle F_{ts} \rangle = \frac{k_z}{2Q_{cl}} \sqrt{A_{free}^2 - A_{cl}^2} = \frac{k_z A_{free}}{2Q_{cl}} \sqrt{1 - \tilde{A}_{cl}}. \quad (16)$$

This equation is equivalent with another common form below [7,17]:

$$A_{cl} = A_{free} \sqrt{1 - 4 \left( \frac{\langle F_{ts} \rangle}{F_{drive}|_{\tilde{\omega}=1}} \right)^2}, \quad (17)$$

where  $F_{drive}$  is given by

$$F_{drive}|_{\tilde{\omega}=1} = \frac{A_{free} k_z}{Q_{cl}}. \quad (18)$$

Fig. 2(a) shows the correlation between the SPR and the converted force at different  $f_{drive}$ . The calculation was performed using typical experimental conditions of HS-AFM:  $k_z = 0.1$  N/m,  $f_0 = 1$  MHz,  $Q_{cl} = 1.5$ , and  $A_{free} = 3$  nm<sub>p-0</sub>. When  $f_{drive}$  is set to  $f_0$ , the curve is nonlinear, and the force rises steeply near SPR = 1. In this condition, even a slight change in the SPR causes a large change in the force, making it difficult to measure with a small force. In contrast, as  $f_{drive}$  is decreased, the force slope becomes smaller and closer to linear, making it possible to measure with a small force. Near the MaxSlope frequency, the force slope is minimized and becomes almost linear. However, as  $f_{drive}$  is further decreased, the slope increases conversely. Since some AM-AFM users excite the cantilever at  $f_{peak}$ , we also examined the calculation result when excited at  $f_{peak}$ . Even in such a case, the force slope is considerably smaller than for excitation at  $f_0$ . This result clearly indicates the conventional force conversion method overestimates the applied force as several times larger than the actual force when excited at  $f_{peak}$  as well as the MaxSlope frequency.

Furthermore, in Fig. 2(b), we also quantified  $f_{\text{drive}}$  dependence of the force (normalized by the value at  $f_0$ ) at SPR = 0.95. We found that a force minimum was observed at a frequency lower than  $f_0$  ( $\tilde{\omega}_{\text{drive}} = 0.58$ , see the arrow). We will call this the MinForce frequency ( $f_{\text{MF}}$ ). We also found that this minimum force appears more prominently as  $Q_{\text{cl}}$  increases. When  $Q_{\text{cl}} = 1.5$ , this minimum force is 1/5 of the force at  $f_0$ . This result suggests that imaging can be performed with the weakest force by exciting at this MinForce frequency.

For example, the conventional equation for  $f_0$  estimates the interaction force at SPR = 0.95 to be 31 pN. This force is substantially stronger than the typical biological binding force of ~10 pN; e.g., the binding force between myosin and F-actin is 15 pN [21]. In contrast, our improved equation estimates the interaction force at SPR = 0.95 to be 6.7 pN when excited at MaxSlope frequency. This force value is below the strength of typical intermolecular bonds, which will reduce tip-induced destructive perturbation of biological samples. Note that the molecular unbinding force increases in proportion to the loading rate. Since the cantilever oscillates at a velocity of >1 mm/s, which corresponds to the loading rate of >10<sup>8</sup> pN/s, the force required to break an intermolecular bond is much larger than the peak force. Therefore, we assumed that the time-averaged force rather than the peak force is the main factor for disturbing the molecular structure.

Furthermore, in Fig. 2(c), we also performed the calculation at a frequency higher than  $f_0$ . In such cases, we found that the applied force is not zero even at SPR = 1. This is consistent with the results in Fig. 1(c,d). When excited at a frequency higher than  $f_0$ , as the tip approaches the surface, the amplitude value increases once due to the effect of the positive frequency shift. Therefore, an excessive force is applied even if SPR = 1, which leads to another adverse effect, i.e., the inversion of image contrast. This is likely to occur under experimental conditions where the squeeze effect is prominent.

However, there are some points to keep in mind when experimentally converting amplitude value into force. In AM-AFM experiments in solution, the amplitude signal gradually decreases as the tip approaches the surface, even if the tip-sample distance is more than a few micrometers.

Therefore, even if the SPR is set to about 0.8, it may be actually performed at  $\text{SPR} > 0.8$ . To accurately estimate the force, it is essential to measure the  $A_{\text{free}}$  by moving the tip away from the surface by 20–30 nm temporarily after approaching.

Furthermore, in solution, when the piezo excitation method is used, the resonance characteristics of the cantilever holder and liquid cell appear instead of the cantilever itself, resulting in spurious peaks [37]. Therefore, when checking optimum  $f_{\text{drive}}$ , it is necessary to determine it in the Brownian noise spectrum. Although this effect must be considered when the force is estimated from the amplitude and phase signals [19,24,25], it does not influence the approximate force conversion equation (Eq. (14)).

We next derive an analytical expression for the MinForce frequency. In Fig. 2(a), the absolute value of the force goes down to zero at  $\text{SPR} = 1$ , however, the force near  $\text{SPR} \sim 1$  correlates with the force slope.

$$\frac{\partial \langle F_{\text{ts}} \rangle}{\partial \tilde{A}_{\text{cl}}} = -\frac{k_z A_{\text{free}}}{2Q_{\text{cl}}} \left[ \frac{\tilde{A}_{\text{cl}} \tilde{\omega}_{\text{drive}}^2}{\sqrt{(1 - \tilde{A}_{\text{cl}}^2) \tilde{\omega}_{\text{drive}}^2 + Q_{\text{cl}}^2 (1 - \tilde{\omega}_{\text{drive}}^2)^2}} + Q_{\text{cl}} (1 - \tilde{\omega}_{\text{drive}}^2) \right]. \quad (19)$$

Then, the conversion coefficient from the amplitude change to force ( $\alpha_{\Delta A \rightarrow F}$ ) is obtained from the force slope at  $\text{SPR} = 1$  as follows:

$$\alpha_{\Delta A \rightarrow F} = \frac{1}{A_{\text{free}}} \lim_{\tilde{A}_{\text{cl}} \rightarrow 1} \frac{\partial \langle F_{\text{ts}} \rangle}{\partial \tilde{A}_{\text{cl}}} = -\frac{k_z}{2Q_{\text{cl}}} \left[ \frac{\tilde{\omega}_{\text{drive}}^2}{Q_{\text{cl}} (1 - \tilde{\omega}_{\text{drive}}^2)} + Q_{\text{cl}} (1 - \tilde{\omega}_{\text{drive}}^2) \right]. \quad (20)$$

This equation is plotted in Fig. 2(d), which bears a close resemblance to that in Fig. 2(c). By solving  $\partial \alpha_{\Delta A \rightarrow F} / \partial \tilde{\omega}_{\text{d}} = 0$ , the MinForce frequency, at which the force becomes minimum, is obtained as follows (see the arrows):

$$\tilde{\omega}_{\text{MF}} = \frac{f_{\text{MF}}}{f_0} = \sqrt{1 - \frac{1}{Q_{\text{cl}}}} \quad (Q_{\text{cl}} \geq 1). \quad (21)$$

Theoretically, the detection sensitivity of conservative forces is maximized at this frequency. However, since excitation is generally performed at the MaxSlope frequency, we next need to verify

which frequency has the greatest advantage.

To predict the MaxSlope frequency, we must solve the second-order differential equation of  $A_{cl}$  (Eq. (9)) as follows;

$$\frac{\partial^2 A_{cl}(\tilde{\omega}_{drive})}{\partial \tilde{\omega}_{drive}^2} = A_0 \left\{ \frac{3\tilde{\omega}_{drive}^2 \left[ 2(1-\tilde{\omega}_{drive}^2) - 1/Q_{cl}^2 \right]^2}{\left[ (1-\tilde{\omega}_{drive}^2)^2 + (\tilde{\omega}_{drive}/Q_{cl})^2 \right]^{5/2}} + \frac{2(1-\tilde{\omega}_{drive}^2) - 1/Q_{cl}^2 - 4\tilde{\omega}_{drive}^2}{\left[ (1-\tilde{\omega}_{drive}^2)^2 + (\tilde{\omega}_{drive}/Q_{cl})^2 \right]^{3/2}} \right\} = 0. \quad (22)$$

Unfortunately, this equation is difficult to solve by elementary functions. However, when  $Q_{cl}$  is sufficiently large ( $Q_{cl} \gg 10$ ),  $A_{cl}$  (Eq. (9)) can be approximated by a Lorentzian function as follows:

$$\lim_{Q_{cl} \rightarrow \infty} A_{cl}(\tilde{\omega}_d) = \frac{A_0}{\sqrt{4(1-\tilde{\omega}_{drive})^2 + 1/Q_{cl}^2}}, \quad (23)$$

which is given by a Taylor series approximation. With this equation, the differential equation above can be analytically solved as follows [20];

$$\tilde{\omega}_{MS} \Big|_{Q_{cl} \gg 10} = \frac{f_{MS}}{f_0} \Big|_{Q_{cl} \gg 10} \approx 1 \pm \frac{1}{\sqrt{8}Q_{cl}} = \begin{cases} 1 + \frac{1}{\sqrt{8}Q_{cl}} & \text{if attractive regime (UMS),} \\ 1 - \frac{1}{\sqrt{8}Q_{cl}} & \text{if repulsive regime (LMS).} \end{cases} \quad (24)$$

In the repulsive regime, the negative sign is used because the frequency shift is positive. This approximation cannot be applied to AM-AFM in liquid because the Q-factor is substantially reduced (1.5 for typical HS-AFM experiments). Therefore, by expanding this approximate solution with a numerically calculated solution of Eq. (22), we obtained a Laurent series approximation equation for the lower MaxSlope ( $\tilde{\omega}_{LMS}$ ) as follows:

$$\tilde{\omega}_{LMS} = 1 - \frac{1}{Q} \left[ \frac{1}{\sqrt{8}} + \frac{0.2148}{Q_{1/2}} - \left( \frac{0.3064}{Q_{1/2}} \right)^2 + \left( \frac{0.2702}{Q_{1/2}} \right)^3 - \left( \frac{0.1947}{Q_{1/2}} \right)^4 \right], \quad (25)$$

where  $Q_{1/2} = Q_{cl} - 1/2$ ,

which is valid for arbitrary  $Q_{cl}$  greater than 0.73. The upper MaxSlope ( $\tilde{\omega}_{UMS}$ ) is shown below:

$$\tilde{\omega}_{\text{UMS}} = 1 + \frac{1}{Q} \left[ \frac{1}{\sqrt{8}} - \frac{0.2191}{Q_{1/4}} + \left( \frac{0.2276}{Q_{1/4}} \right)^2 - \left( \frac{0.252}{Q_{1/4}} \right)^3 + \left( \frac{0.2107}{Q_{1/4}} \right)^4 \right], \quad (26)$$

$$\text{where } Q_{1/4} = Q_{\text{cl}} - 1/4,$$

which is valid for arbitrary  $Q_{\text{cl}}$  greater than 0.5. Hereafter, we define the MaxSlope frequency as the lower MaxSlope because we focus on liquid AM-AFM.

We next compare  $Q_{\text{cl}}$  dependence of the MinForce and MaxSlope frequencies. In Fig. 2(e), as  $Q_{\text{cl}}$  decreases, the MinForce frequency steeply falls down to 0 even at  $Q_{\text{cl}} = 1$  while the MaxSlope frequency is maintained above 0.4 at  $Q_{\text{cl}} > 1$ . In contrast, the force shows no significant difference over all the Q-factor range (Fig. 2(f)). The cantilever should be driven at the highest possible frequency because the feedback bandwidth and the sensitivity to energy dissipation decrease as  $f_{\text{drive}}$  decreases. Therefore, in practice, we can conclude that excitation at the MaxSlope frequency provides the best force detection sensitivity.

As shown in Fig. 2(a), when excited at MaxSlope, the force linearly increases with respect to the amplitude reduction especially at SPR  $\sim 1$ , and is approximated by

$$\langle F_{\text{ts}} \rangle \approx \alpha_{\Delta A \rightarrow F} \Delta A_{\text{ts}}. \quad (27)$$

By setting the MaxSlope frequency for  $f_{\text{drive}}$  and an HS-AFM typical value of  $Q_{\text{cl}} = 1.5$ , in Eq. (20),  $\alpha_{\Delta A \rightarrow F}$  is approximately expressed by

$$\alpha_{\Delta A \rightarrow F} \approx -457 \cdot k_z \quad [\text{pN/nm}]. \quad (28)$$

In this condition, a practical expression of the force can be obtained as

$$\begin{aligned} \langle F_{\text{ts}} \rangle &\approx -457 \cdot k_z \Delta A_{\text{ts}} \\ &= 457 \cdot k_z A_{\text{free}} (1 - \tilde{A}_{\text{cl}}) \quad [\text{pN}]. \end{aligned} \quad (29)$$

By setting other HS-AFM typical values,  $k_z = 0.1$  N/m and  $A_{\text{free}} = 3$  nm<sub>p=0</sub>, a more practical expression can be obtained as

$$\langle F_{\text{ts}} \rangle \approx 137 \cdot (1 - \tilde{A}_{\text{cl}}) \quad [\text{pN}]. \quad (30)$$

By using this equation, for example, we can easily estimate the tip-sample interaction force as 6.9

and 13.7 pN for SPR = 0.95 and 0.9, respectively. The force of 6.9 pN is consistent with the value of 6.7 pN that was predicted by nonlinear equation Eq. (14).

To verify the applicability of these approximations, we also numerically simulated the interaction force as a function of the tip-sample distance based on the Hertz equation for contact between a sphere and an infinite plane as follows [27,28,38-40];

$$F_{\text{Hertz}} = \frac{4E^*}{3} R_{\text{tip}}^{1/2} (-\delta)^{3/2}, \quad (31)$$

where  $R_{\text{tip}}$  and  $\delta$  are the radius of curvature of the tip and indentation depth, respectively, and  $E^*$  is the reduced Young's modulus, which is expressed by

$$E^* = \left( \frac{1-\nu_s^2}{E_s} + \frac{1-\nu_{\text{tip}}^2}{E_{\text{tip}}} \right)^{-1}, \quad (32)$$

where  $\nu$  and  $E$  are the Poisson's ratio and Young's modulus, and the subscript s and tip denote the sample and tip, respectively. We simulated the equation of motion (Eq. (1)) using the velocity Verlet algorithm with  $R_{\text{tip}}$  and  $A_{\text{free}}$  of 5 nm and 3 nm<sub>p=0</sub>, respectively, and calculated the force from the time averaged deflection. Because we normally use an electron-beam deposited tip [10], we assumed  $\nu_{\text{tip}}$  and  $E_{\text{tip}}$  of 0.3 and 100 GPa, respectively, according to previous descriptions of a carbon nanopillars [41,42]. For the sample, we assumed  $\nu_s$  of 0.33, which is typical for globular proteins [43,44], and varied  $E_s$  in the range of 1–1000 MPa. In Fig. 2(g,h), good agreements were obtained in both the MaxSlope and resonance frequencies when the SPR was 0.5 or more on the surface with  $E_s$  of more than 100 MPa. However,  $E_s$  of 10 MPa requires an SPR greater than 0.8, and  $E_s$  of 1 MPa requires an SPR greater than 0.9 in order to obtain good agreement.

Structural proteins, which are the most amenable to HS-AFM observation, generally have  $E_s$  on the order of GPa. Although lipid membranes and liposomes in a fluid phase have  $E_s$  of several MPa, the apparent  $E_s$  in AFM experiments increases to one order higher than the real value because of the substrate bottom effect [39,40]. Therefore, it is rare that observation target has  $E_s$  of less than 10 MPa. Furthermore, in nondestructive biomolecular imaging, the SPR is normally set to 0.9 or

more, suggesting that this force conversion method can be adapted to a wide range of systems.

### 3. Conversion from Interaction Depth to Amplitude

The equation derived above works well when the feedback error is sufficiently small. However, when observing a large structure, the feedback error often becomes considerably large uphill of the structure, which causes an additional force. Therefore, we discuss below how the additional force differs depending on  $f_{\text{drive}}$ . As illustrated in Fig. 3(a),  $\Delta A_{\text{ts}}$  can be calculated by the average of the decrease in the peak top ( $\Delta A_{\text{top}}$ ) and peak bottom ( $\Delta A_{\text{bot}}$ ) as follows;

$$\begin{aligned}\Delta A_{\text{ts}} &= \frac{1}{2}(\Delta A_{\text{bot}} + \Delta A_{\text{top}}) \\ \therefore \Delta A_{\text{top}} &= 2\Delta A_{\text{ts}} - \Delta A_{\text{bot}}.\end{aligned}\tag{33}$$

Meanwhile, the average displacement of the cantilever  $\Delta\langle z \rangle$  can be calculated from the difference between  $\Delta A_{\text{top}}$  and  $\Delta A_{\text{bot}}$  as follows:

$$\begin{aligned}\Delta\langle z \rangle &= \frac{1}{2}[A_{\text{free}} + \Delta A_{\text{top}} - (A_{\text{free}} + \Delta A_{\text{bot}})] \\ &= \frac{1}{2}(\Delta A_{\text{top}} - \Delta A_{\text{bot}}).\end{aligned}\tag{34}$$

Note that  $\Delta A_{\text{ts}}$  and  $\Delta\langle z \rangle$  take negative and positive values, respectively. Combining these equations, we obtain

$$\Delta\langle z \rangle = \Delta A_{\text{ts}} - \Delta A_{\text{bot}}.\tag{35}$$

When the sample surface is sufficiently rigid and the tip hardly penetrates the surface,  $\Delta A_{\text{bot}}$  approximately equals the interaction depth  $\Delta z_{\text{int}}$  (tip-sample distance relative to the distance where  $\Delta A_{\text{ts}}$  starts to decrease) as follows:

$$\Delta A_{\text{bot}} \approx \Delta z_{\text{int}}.\tag{36}$$

Therefore, we obtain

$$\Delta A_{\text{ts}} = \Delta z_{\text{int}} + \Delta\langle z \rangle.\tag{37}$$



The average force divided by  $k_z$  equals  $\Delta\langle z \rangle$ , and hence it is expressed as follows:

$$\Delta\langle z \rangle = \frac{\langle F_{ts} \rangle}{k_z} = -\frac{1}{2Q_{cl}} \left[ \frac{\tilde{\omega}_{drive}^2}{Q_{cl}(1-\tilde{\omega}_{drive}^2)} + Q_{cl}(1-\tilde{\omega}_{drive}^2) \right] \Delta A_{ts}. \quad (38)$$

Combining these two equations, we obtain the equation below:

$$\begin{aligned} \Delta A_{ts} &= \left\{ 1 + \frac{1}{2Q_{cl}} \left[ \frac{\tilde{\omega}_{drive}^2}{Q_{cl}(1-\tilde{\omega}_{drive}^2)} + Q_{cl}(1-\tilde{\omega}_{drive}^2) \right] \right\}^{-1} \Delta z_{int} \\ &= \alpha_{\Delta z \rightarrow \Delta A} \Delta z_{int} \end{aligned} \quad (39)$$

where  $\alpha_{\Delta z \rightarrow \Delta A}$  is the conversion coefficient from  $\Delta z_{int}$  to  $\Delta A_{ts}$ .

Fig. 3(b) shows the  $Q_{cl}$  dependence of  $\alpha_{\Delta z \rightarrow \Delta A}$  when excited at the MaxSlope frequency, where  $\alpha_{\Delta z \rightarrow \Delta A}$  takes a value between 0.65 and 1. When  $Q_{cl}$  is small,  $\alpha_{\Delta z \rightarrow \Delta A}$  is close to 0.65 because  $\Delta A_{top}$  is only slightly decreased by the surface interaction. When  $Q_{cl}$  is high,  $\alpha_{\Delta z \rightarrow \Delta A}$  asymptotically leads to the value of 1 because both  $\Delta A_{bot}$  and  $\Delta A_{top}$  decrease simultaneously.

Furthermore, by substituting this into the conversion equation from amplitude to force (Eq. (20)), we obtain the equation for directly calculating the force from the feedback error as follows:

$$\begin{aligned} \langle F_{ts} \rangle &= \alpha_{\Delta A \rightarrow F} \Delta A_{ts} \\ &= \alpha_{\Delta z \rightarrow F} \Delta z_{int} \\ &= (\alpha_{\Delta A \rightarrow F} \cdot \alpha_{\Delta z \rightarrow \Delta A}) \Delta z_{int} \\ &= \frac{-k_z \Delta z_{int}}{1 + \left\{ \frac{1}{2Q_{cl}} \left[ \frac{\tilde{\omega}_{drive}^2}{Q_{cl}(1-\tilde{\omega}_{drive}^2)} + Q_{cl}(1-\tilde{\omega}_{drive}^2) \right] \right\}^{-1}}, \end{aligned} \quad (40)$$

where  $\alpha_{\Delta z \rightarrow F}$  is the conversion coefficient from  $\Delta z_{int}$  to force, which takes a negative value.

By assuming an excitation at the MaxSlope frequency and using a typical  $Q_{cl}$  in HS-AFM measurements of 1.5,  $\alpha_{\Delta z \rightarrow \Delta A}$  takes a value of 0.686 regardless of the  $A_{free}$  value. Therefore, we obtain a practical expression as follows:

$$\Delta A_{ts} = 0.686 \cdot \Delta z_{int} \quad [\text{nm}], \quad (41)$$

$$\alpha_{\Delta z \rightarrow F} \approx -314 \cdot k_z \quad [\text{pN/nm}]. \quad (42)$$

In this condition, a practical expression of the force can be obtained as

$$\langle F_{ts} \rangle = -314 \cdot k_z \Delta z_{\text{int}} \quad [\text{pN}]. \quad (43)$$

This equation indicates that the effective  $k_z$  can be reduced to  $\sim 1/3$  of the actual  $k_z$  by exciting the cantilever at the MaxSlope frequency, reducing tip-sample force and ameliorating tip-mediated sample disruption and perturbation.

To confirm the validity of these equations, we compared them with the results of numerical calculations based on the Hertz model under the same conditions as those in Fig. 2(g,h). In Fig. 3(c,d), we found that the analytical result (yellow broken line) generally matched well when  $E_s$  is 100 MPa or more in both the force and amplitude curves. This range encompasses the  $E_s$  of most structural proteins, which is usually on the order of GPa. Under conditions where  $E_s$  is 10 MPa or less, this approximation slightly overestimates the force.

We also compared the results when excited at  $f_0$  in Fig. 3(e,f). When  $E_s$  is greater than 100 MPa, the force increased faster, plateauing several times greater than for the analytical solution of MaxSlope (yellow broken line) at a shallow interaction depth of  $\sim 1$  nm. However, the amplitude decreased almost linearly as  $\Delta z_{\text{int}}$  decreased, similar to the analytical solution of MaxSlope. This means that the force cannot be accurately determined from the distance dependence of the amplitude value alone, and therefore  $f_{\text{drive}}$  must be recorded in advance.

Furthermore, in Fig. 3(c), when  $\Delta z_{\text{int}}$  becomes smaller than  $-A_{\text{free}}$ , the force increased steeply and deviated significantly from the approximation (yellow broken line). We found that the force slope at the distance of  $\Delta z_{\text{int}} \leq -A_{\text{free}}$  can be well fitted by  $k_z$  as follows (cyan broken line):

$$\langle F_{ts} \rangle = -k_z (\Delta z_{\text{int}} + A_{\text{free}}) \quad \text{if } \Delta z_{\text{int}} \leq -A_{\text{free}}, \quad (44)$$

which indicates that the force becomes as strong as that in the contact mode.

In addition, we also found that, when  $E_s$  is 1 GPa or more, the numerical simulation results at the arbitrary distance can be fitted by

$$\langle F_{ts} \rangle = \max \left\{ \alpha_{\Delta z \rightarrow F} \Delta z_{\text{int}}, -k_z (\Delta z_{\text{int}} + A_{\text{free}}) \right\}. \quad (45)$$

This analysis suggests that the cantilever oscillation amplitude should be set to be greater than the height of the molecules in order to minimize perturbation during imaging. Conversely, if the amplitude value is too large, it becomes susceptible to noise and fluctuation in the excitation efficiency of the cantilever. Therefore, generally, as for HS-AFM observations, an amplitude value equivalent to the height of the molecules is used with an upper limit of 10 nm.

## Conclusions

In this study, we succeeded in elucidating a previously unaddressed issue in that the force converted from the amplitude value in AM-AFM is substantially larger than the typical molecular binding forces. By analyzing the equation of motion of the cantilever, we revealed that whereas AM-AFM experiments are generally performed with excitation at the MaxSlope frequency, the conventional conversion equation is only valid for the excitation at  $f_0$ . This discrepancy results in a 5-fold overestimation of the actual force. The theoretical formulation shown here is valid for the attractive forces in ambient conditions as well as repulsive forces in liquid conditions. It is expected to not only provide a basis for further increasing the speed of HS-AFM via the calculation of the minimum detectable force, but also be useful in general material research fields that use AM-AFM.

## Figs

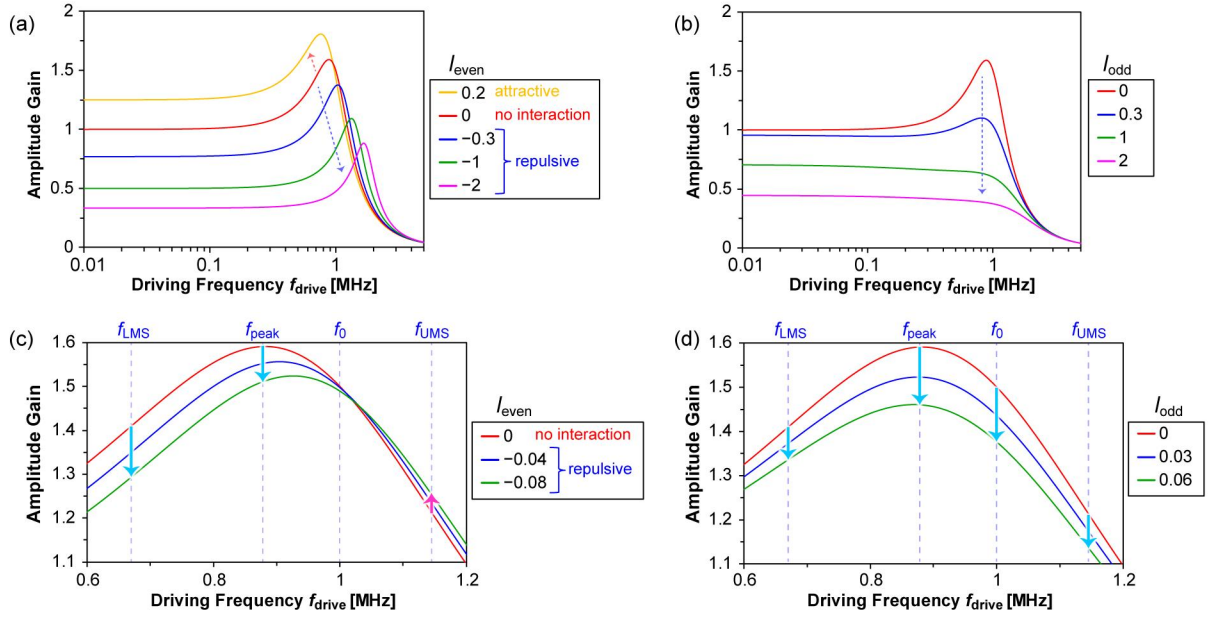


**Figure. 1** | (a,b) Calculated frequency characteristics of the resonance peak of the cantilever amplitude signal dependent on  $I_{even}$  (a) and  $I_{odd}$  (b). Positive and negative values of  $I_{even}$  correspond to the attractive and repulsive forces, respectively. (c,d) Enlarged frequency characteristics of the resonance peak of the cantilever amplitude signal dependent on  $I_{even}$  (c) and  $I_{odd}$  (d). The vertical broken lines indicate the amplitude variation at several characteristic frequencies:  $f_{LMS}$ ,  $f_{peak}$ ,  $f_0$ , and  $f_{UMS}$  represent the lower MaxSlope, peak, resonance, and upper MaxSlope frequencies, which are 0.67, 0.88, 1, and 1.14 MHz, respectively. All the data are calculated with  $Q_{cl} = 1.5$ , which is typical for an HS-AFM experiment.

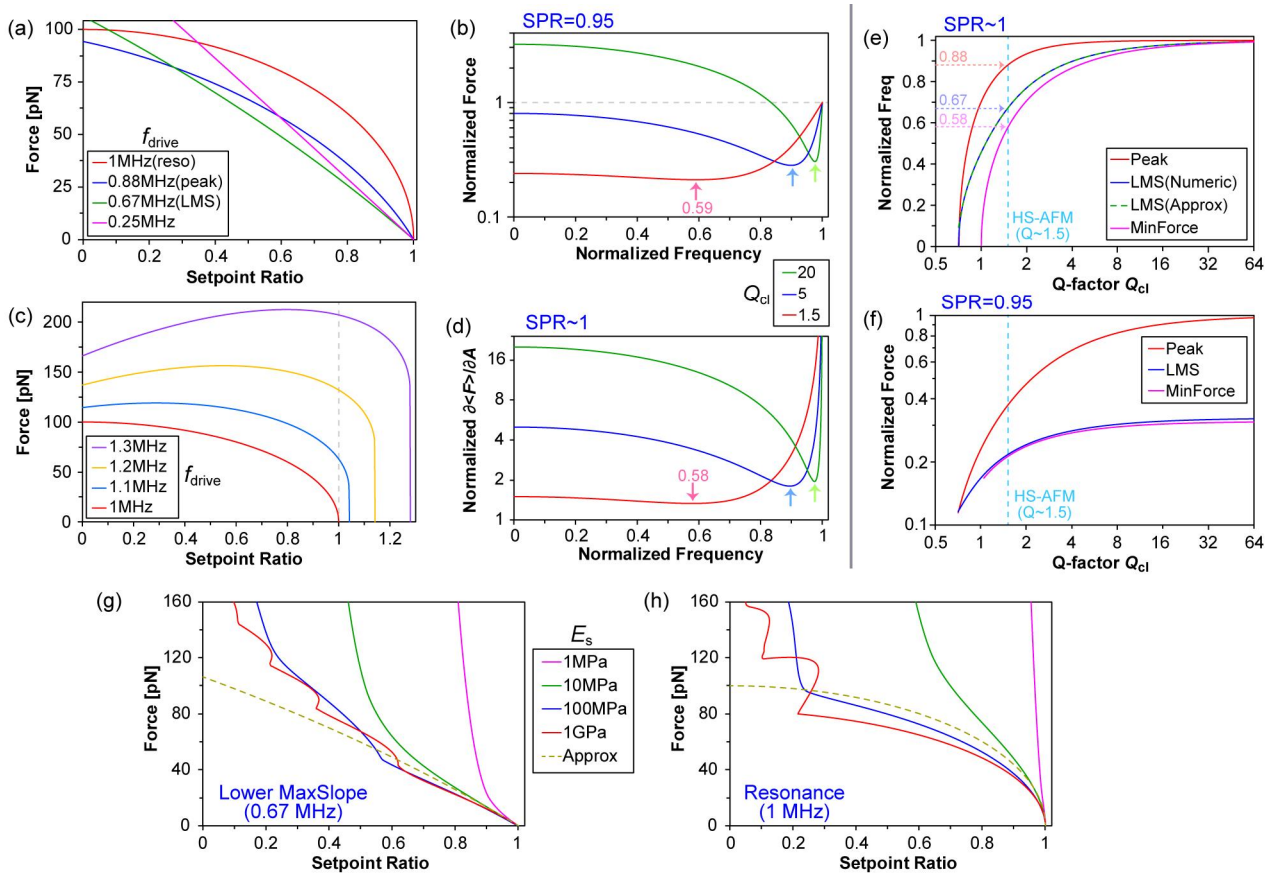


**Figure. 2** | **(a,b)** Setpoint dependence of average force when the excitation frequency is lower (a) and higher (b) than the resonance frequency. In the legend, reso, peak, and LMS represent resonance, peak, and lower MaxSlope frequencies, respectively. **(c)** Excitation frequency dependence of average force ( $SPR = 0.95$ ) normalized by those at the resonance. **(d)** Excitation frequency dependence of normalized  $\partial F/\partial A$  ( $SPR = 1$ ) at different  $Q_{cl}$ . The arrows in (b,d) indicate the MinForce frequencies for each  $Q_{cl}$ . **(e,f)**  $Q$ -factor dependence of normalized frequency and force ( $SPR = 0.95$ ) of MaxSlope and MinForce. **(g,h)** Numerical simulation and approximation results of setpoint dependence of force when the excitation frequency is at the MaxSlope (g) and resonance (h) frequencies.

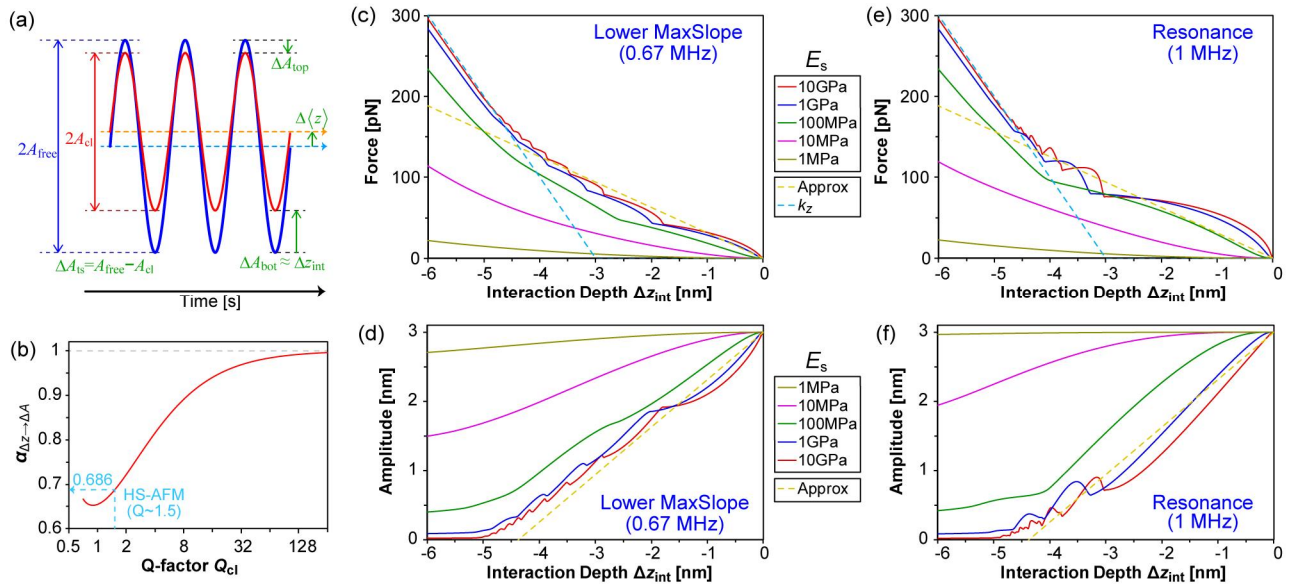


**Figure. 3** | (a) Schematic diagram for deriving a theoretical equation for simulating the decrease in oscillation amplitude from the interaction depth. (b) Q-factor dependence of conversion factor from  $\Delta z_{int}$  to  $\Delta A_{ts}$ . (c–f) Interaction depth dependence of the average force (c,e) and oscillation amplitude (d,f) on sample with different Young's modulus when excited at the MaxSlope frequency (c,d) and resonance (e,f) frequencies.

## **Acknowledgments**

We thank Dr. Steven J. McArthur for critical reading and the English language improvement of the paper. This work was supported by PRESTO, Japan Science and Technology Agency (JST) [JPMJPR20E3 and JPMJPR23J2 to K.U.]; CREST, JST [JPMJCR1762 to N.K.]; and KAKENHI, Japan Society for the Promotion of Science [21K04849 (to K.U.), 26119003, and 20H00327 (to N.K.)].

## **Author contributions**

K. U. constructed the theories and wrote the manuscript; K. K. supported the study; and N. K. supervised the study.

## **Data availability**

The data that support the findings of this study are available from the corresponding author upon reasonable request.

## References

- [1] R. Giridharagopal, L. Q. Flagg, J. S. Harrison, M. E. Ziffer, J. Onorato, C. K. Luscombe, and D. S. Ginger, *Nat. Mater.* **16**, 737 (2017).
- [2] A. F. Payam and A. Passian, *Sci. Adv.* **9**, eadg8292 (2023).
- [3] V. V. Korolkov, A. Summerfield, A. Murphy, D. B. Amabilino, K. Watanabe, T. Taniguchi, and P. H. Beton, *Nat. Commun.* **10**, 1537 (2019).
- [4] S. Chiodini *et al.*, *ACS Nano* **16**, 7589 (2022).
- [5] Y. C. Lin, Y. R. Guo, A. Miyagi, J. Levring, R. MacKinnon, and S. Scheuring, *Nature* **573**, 230 (2019).
- [6] N. Chiaruttini, L. Redondo-Morata, A. Colom, F. Humbert, M. Lenz, S. Scheuring, and A. Roux, *Cell* **163**, 866 (2015).
- [7] R. Garcia, R. Magerle, and R. Perez, *Nat. Mater.* **6**, 405 (2007).
- [8] S. Shi, D. Guo, and J. B. Luo, *J. Phys. D: Appl. Phys.* **50**, 415307 (2017).
- [9] J. Snijder *et al.*, *Nat. Chem.* **5**, 502 (2013).
- [10] T. Ando, T. Uchihashi, and S. Scheuring, *Chem. Rev.* **114**, 3120 (2014).
- [11] K. Umeda, S. J. McArthur, and N. Kodera, *Microscopy* **72**, 151 (2023).
- [12] T. Fukui, T. Uchihashi, N. Sasaki, H. Watanabe, M. Takeuchi, and K. Sugiyasu, *Angew. Chem. Int. Edit.* **57**, 15465 (2018).



- [13] C. Ganser and T. Uchihashi, *Microscopy* **73**, 14 (2024).
- [14] A. P. Nievergelt, N. Banterle, S. H. Andany, P. Gonczy, and G. E. Fantner, *Nat. Nanotechnol.* **13**, 696 (2018).
- [15] W. S. Klug, W. H. Roos, and G. J. L. Wuite, *Phys. Rev. Lett.* **109**, 168104 (2012).
- [16] B. Voigtländer, in *Atomic Force Microscopy 2nd ed.* (Springer, Berlin, 2019), p. 264 & 290.
- [17] A. San Paulo and R. Garcia, *Phys. Rev. B* **64**, 193411 (2001).
- [18] T. R. Rodriguez and R. Garcia, *Appl. Phys. Lett.* **82**, 4821 (2003).
- [19] H. Hölscher, *Appl. Phys. Lett.* **89**, 123109 (2006).
- [20] Y. Martin, C. C. Williams, and H. K. Wickramasinghe, *J. Appl. Phys.* **61**, 4723 (1987).
- [21] H. Nakajima, Y. Kunioka, K. Nakano, K. Shimizu, M. Seto, and T. Ando, *Biochem. Biophys. Res. Commun.* **234**, 178 (1997).
- [22] S. Uchimura, Y. Oguchi, M. Katsuki, T. Usui, H. Osada, J. Nikawa, S. Ishiwata, and E. Muto, *EMBO J.* **25**, 5932 (2006).
- [23] L. S. Shlyakhtenko, A. Y. Lushnikov, and Y. L. Lyubchenko, *Biochemistry* **48**, 7842 (2009).
- [24] M. H. Lee and W. H. Jhe, *Phys. Rev. Lett.* **97**, 036104 (2006).
- [25] A. J. Katan, M. H. van Es, and T. H. Oosterkamp, *Nanotechnology* **20**, 165703 (2009).
- [26] T. R. Albrecht, P. Grütter, D. Horne, and D. Rugar, *J. Appl. Phys.* **69**, 668 (1991).
- [27] H. Hölscher, D. Ebeling, and U. D. Schwarz, *J. Appl. Phys.* **99**, 084311 (2006).
- [28] H. Hölscher and U. D. Schwarz, *Appl. Phys. Lett.* **89**, 073117 (2006).

- [29] U. Dürig, New J. Phys. **2**, 5 (2000).
- [30] B. A. Bircher, R. Krenger, and T. Braun, EPJ Tech. Instrum. **1**, 10 (2014).
- [31] A. San Paulo and R. Garcia, Phys. Rev. B **66**, 041406 (2002).
- [32] Asylum MFP 3D User Guide, <https://www.afmhelp.com/docs/manuals/mfp3dmanual.pdf>  
(Accessed July 1, 2024)
- [33] JPK NanoWizard 3 User Manual,  
<https://www.nanophys.kth.se/nanolab/afm/jpk/manuf-manuals/usermanual.4.2.pdf> (Accessed  
July 1, 2024)
- [34] Veeco MultiMode SPM Instruction Manual,  
[https://www.cigs.unimo.it/cigsdownloads/labs/afm2/manuali\\_lettura/multimode\\_manual\\_rev\\_b.pdf](https://www.cigs.unimo.it/cigsdownloads/labs/afm2/manuali_lettura/multimode_manual_rev_b.pdf) (Accessed July 1, 2024)
- [35] Park Systems web site,  
<https://www.parksystems.com/jp/jp/park-spm-modes/91-standard-imaging-mode/2204-tapping-mode> (Accessed July 1, 2024)
- [36] Agilent Technologies 5500 Scanning Probe Microscope User's Guide,  
[https://afmhelp.com/docs/manuals/agilent\\_5500\\_user\\_manual\\_revB.pdf](https://afmhelp.com/docs/manuals/agilent_5500_user_manual_revB.pdf) (Accessed July 1,  
2024)
- [37] K. Umeda, K. Kobayashi, K. Matsushige, and H. Yamada, Appl. Phys. Lett. **101**, 123112  
(2012).

- [38] D. Ebeling, H. Hölscher, and B. Anczykowski, *Appl. Phys. Lett.* **89**, 203511 (2006).
- [39] V. G. Gisbert and R. Garcia, *ACS Nano* **15**, 20574 (2021).
- [40] E. K. Dimitriadis, F. Horkay, J. Maresca, B. Kachar, and R. S. Chadwick, *Biophys. J.* **82**, 2798 (2002).
- [41] J. Fujita, M. Ishida, T. Sakamoto, Y. Ochiai, T. Kaito, and S. Matsui, *J. Vac. Sci. Technol. B* **19**, 2834 (2001).
- [42] K. Nakamatsu, M. Nagase, J. Y. Igaki, H. Namatsu, and S. Matsui, *J. Vac. Sci. Technol. B* **23**, 2801 (2005).
- [43] M. Radmacher, M. Fritz, J. P. Cleveland, D. A. Walters, and P. K. Hansma, *Langmuir* **10**, 3809 (1994).
- [44] D. P. Kharakoz, *Biophys. J.* **79**, 511 (2000).